Ternary Nitrides

DOI: 10.1002/anie.200805394

Highly Conductive Films of Layered Ternary Transition-Metal Nitrides**

Hongmei Luo, Haiyan Wang, Zhengxing Bi, Guifu Zou, T. Mark McCleskey, Anthony K. Burrell, Eve Bauer, Marilyn E. Hawley, Yongqiang Wang, and Quanxi Jia**

Metal nitrides exhibit a number of important properties, such as superconductivity, catalytic activity, unusual magnetic properties, and high hardness and mechanical strength.[1–7] Great efforts have been made in exploring new ternary and higher-order metal nitrides since the 1990s. However, the intrinsic physical properties of many ternary metal nitrides have not been well-studied because of the synthetic challenges in preparing single-phase ternary metal nitrides. For example, $BaZrN_2$ (BZN), $BaHfN_2$ (BHN), and their solid solution $Ba(Hf_{1-x}Zr_x)N_2$ have only been prepared by a solid-state reaction approach.[8–10] These ternary metal nitride powders are known to contain impurities such as the binary nitrides ZrN and HfN.[8–10] The presence of impurities makes it very difficult to study the intrinsic properties of the ternary nitrides. Herein, we report the preparation of epitaxial thin films of the ternary metal nitrides BZN and BHN on (001) $SrTiO_3$ (STO) substrates by a chemical-solution approach to polymer-assisted deposition (PAD).[11–13] The successful growth of single-phase ternary metal nitrides by a controllable and reproducible synthesis route makes it possible to study the fundamental physical properties of these materials. This achievement is also a tremendous leap forward toward the utilization of these materials for technological applications.

It is known that both BZN and BHN crystallize in the layered $KCoO_2$ structure type in space group $P4/nmm$ ($a_{BZN} = 0.416297$, $c_{BZN} = 0.840318$ nm for BZN; $a_{BHN} = 0.41279$, $c_{BHN} = 0.83816$ nm for BHN). In BZN and BHN, the Ba^{2+} cations sit between layers of edge-sharing square-pyramidal $[ZrN_2]^{2-}$ or $[HfN_2]^{2-}$ anions.[8–10] The relatively small in-plane lattice mismatch between these metal nitrides and STO ($a_{STO} = 0.3901$ nm) makes it possible to epitaxially grow these materials as films. Figure 1 shows X-ray diffraction (XRD) patterns obtained from θ–2θ and ϕ scans of BZN and BHN films on STO substrates, after the films were annealed at 1000 °C for 1 h. The appearance of (002) and (004) diffraction peaks from the tetragonal BZN or BHN film together with (001) and (002) diffraction peaks from the STO substrate indicates that the films are preferentially oriented with the *c* axis perpendicular to the substrate surface. Note that no other phases are detected. In contrast, ternary metal nitrides formed by a ceramic process often contain binary nitrides.[8–10]

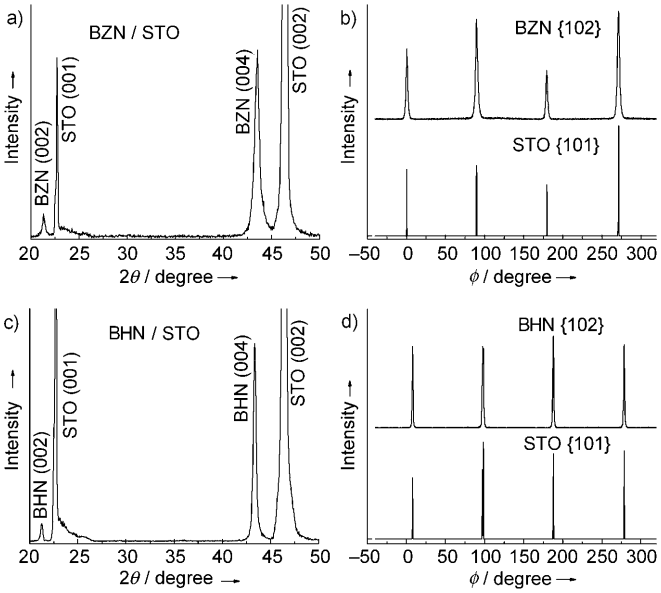

Figure 1. XRD patterns obtained from a) a θ–2θ scan of a BZN film on STO, b) ϕ scans of the (102) diffraction peak of BZN and the (101) diffraction peak of STO, c) a θ–2θ scan of a BHN film on STO, and d) ϕ scans of the (102) diffraction peak of BHN and the (101) diffraction peak of STO.

We measured carbon and oxygen contamination in the films with resonant Rutherford backscattering spectrometry (RBS). The films do contain some carbon and oxygen, but probably less than 10 %. Note that the analysis of carbon and oxygen on the basis of RBS is quite difficult without reliable standards.

The in-plane relative orientation of each film and the substrate was determined from XRD patterns obtained from

[*] Dr. H. M. Luo, Dr. G. F. Zou, Dr. T. M. McCleskey, Dr. A. K. Burrell, E. Bauer, Dr. Q. X. Jia
Materials Physics and Applications Division
Los Alamos National Laboratory, Los Alamos, NM 87545 (USA)
Fax: (+1) 505-665-3164
E-mail: hluo@lanl.gov
qxjia@lanl.gov
Dr. H. M. Luo
Department of Chemical Engineering
New Mexico State University, Las Cruces, NM 88003 (USA)
Dr. H. Wang, Z. Bi
Department of Electrical and Computer Engineering
Texas A&M University, College Station, TX 77843 (USA)
Dr. M. E. Hawley, Dr. Y. Wang
Materials Science and Technology Division
Los Alamos National Laboratory, Los Alamos, NM 87545 (USA)

[**] We gratefully acknowledge the support of the U.S. Department of Energy (DOE) through the LANL/LDRD Program, the DOE EE-RE Solid State Lighting Program, and the NSF/DMR Ceramic Program (NSF 0709831).

ϕ scans of the (102) diffraction peak of BZN or BHN and the (101) diffraction peak of STO, respectively. The epitaxial relationships between the films and the substrate can be generally described as $(001)_{film}||(001)_{STO}$ and $[102]_{film}||[101]_{STO}$. Average full-width-at-half-maximum (FWHM) values of 2.0° for the BZN film and of 1.5° for the BHN film, as compared to 0.7° for the STO substrate, indicate that the films are of good epitaxial quality. Note that this is the first report of the growth of single-phase epitaxial BZN and BHN films. The lattice parameters of these epitaxial films, calculated from the (004) and (102) diffraction peaks, are $a_{BZN} = 0.407$ and $c_{BZN} = 0.852$ nm for the BZN film, and $a_{BHN} = 0.411$ and $c_{BHN} = 0.839$ nm for the BHN film. Compared with those of the bulk materials, the in-plane lattice parameters of the films are each slightly smaller, while the out-of-plane lattice parameters are each slightly larger. This finding is understandable, considering that such epitaxial films are under compressive strain.

The surface morphology and surface roughness of the films were investigated by scanning electron microscopy (SEM) and atomic force microscopy (AFM). The films are dense and smooth, without any detectable microcracks. AFM images of BZN and BHN films grown on STO substrates are shown in Figure 2. The root-mean-square (rms) surface roughness, measured from a 1 μm × 1 μm area of the AFM image, was 2 nm for the BZN film and 2.14 nm for the BHN film.

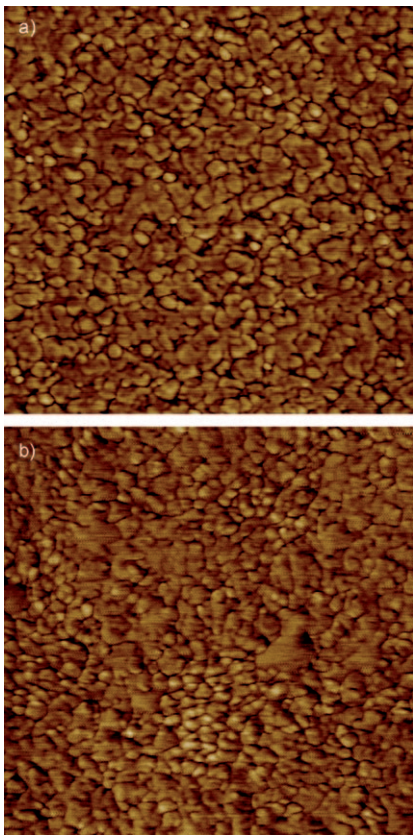

Figure 2. AFM images (1 μm × 1 μm) of a) a BZN film on STO and b) a BHN film on STO.

Figure 3 shows a bright-field cross-section transmission electron microscopy (TEM) image of a BZN film (38 nm thick) on an STO substrate, as well as high-resolution (HR) TEM images of BZN and BHN films on STO substrates. For both the BZN and the BHN films, the interface between the film and the substrate is flat and clean, without any indication of intermixing. The corresponding selected-area electron diffraction (SAED) patterns taken from the interface (Figure 3a, inset for BZN; Figure 3c, inset for BHN) confirm the epitaxial growth of tetragonal BZN and BHN films on the STO substrates, as evidenced by the distinct diffraction spots from each of the films and the substrate. The epitaxial relationships between each of the films and the substrate

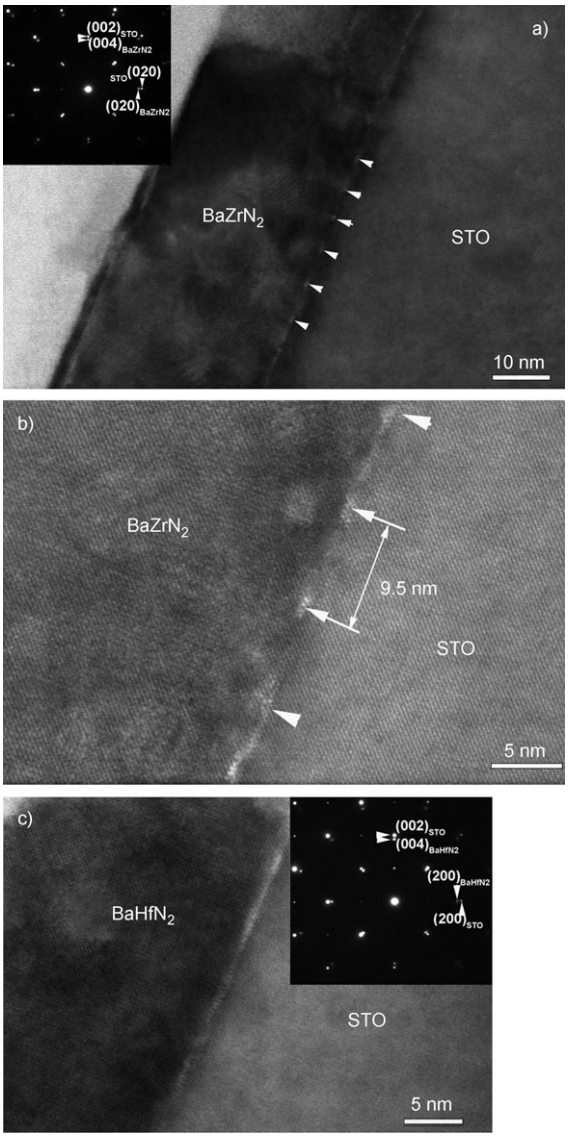

Figure 3. a) A bright-field cross-section TEM image of a BZN film (38 nm thick) on STO (inset: the corresponding SAED pattern from the interface between BZN and STO). HRTEM images of b) the interface between BZN and STO, and c) the interface between BHN and STO (inset: the corresponding SAED pattern from the interface between BHN and STO). The arrows along the interface of BZN and STO in (a) and (b) indicate a very ordered misfit dislocation. See text for details.

determined from the SAED patterns are consistent with those determined from the XRD patterns. Note that the SAED patterns of each of the films demonstrate the epitaxial growth of a single-phase material, as no diffraction spots arising from other phases are detected.

More interestingly, uniformly distributed misfit dislocations (marked with arrows) are observed along the interface of the BZN film and the STO substrate. The lattice misfit between BZN and STO is 4.3%. The corresponding misfit-dislocation spacing d_m, calculated according to $d_m = d_1 d_2/(d_1 - d_2)$, where $d_1 = a_{BZN} = 0.407$ nm and $d_2 = a_{STO} = 0.3901$ nm, is 9.4 nm, which is consistent with the misfit-dislocation spacing of 9.5 nm measured from Figure 3b. The domain-matching numbers of planes are $d_m/d_1 = 9.4/0.407 = 23$ for the BZN film and $d_m/d_2 = 9.4/0.3901 = 24$ for the STO substrate. Thus, the domain-matching relationship between the film and the substrate is $23\,a_{BZN}$ to $24\,a_{STO}$. Similarly, the BHN film on the STO substrate has a lattice mismatch of 5.3%, which results in a misfit-dislocation spacing of 7.7 nm and a domain-matching relationship of $19\,a_{BHN}$ to $20\,a_{STO}$.

Superconducting transition temperatures of 9.5 and 8.9 K have been reported for BZN and BHN powders, respectively.[8–10] However, ZrN and HfN are also known to be superconducting, with transition temperatures of 10 and 8.83 K, respectively.[14,15] Since the powders of the ternary nitrides contained binary nitride impurities,[8–10] it is reasonable to ask the following question: was the superconductivity reported for these ternary nitride samples an intrinsic property of these materials, or did it arise from the binary nitride impurities? The growth of single-phase epitaxial films of BZN and BHN allows us to study the intrinsic properties of these ternary nitride materials.

Figure 4 shows the temperature dependence of the resistivity of BZN and BHN films on STO substrates, measured by the standard four-probe technique. Both films show metallic-like resistivity–temperature behavior from 5 to 300 K. At 5 K, the resistivity is as low as $0.0026 \times 10^{-4}\,\Omega$ cm for BZN and $0.003 \times 10^{-4}\,\Omega$ cm for BHN. Nevertheless, no superconducting transition is observed down to 5 K for either the BZN or the BHN film.

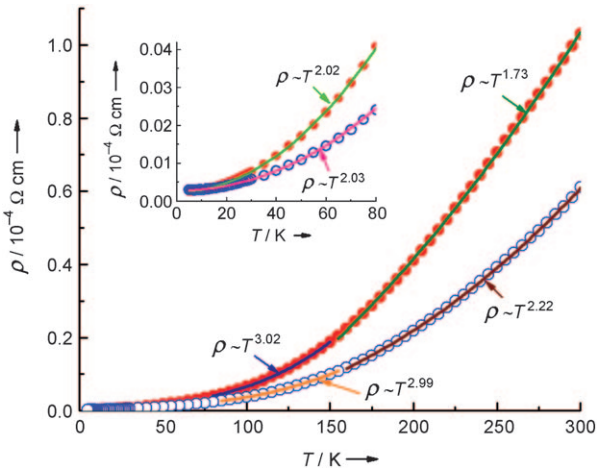

Figure 4. Temperature dependence of the resistivity ρ of BZN (red circles) and BHN (blue circles) on STO with the fits of $\rho(T) = \rho_0 + AT^m$ (solid lines). See text for details.

This result is further confirmed by the temperature dependence of the magnetization of BZN and BHN films on STO substrates, measured on a superconducting quantum interference device (SQUID) magnetometer. It is possible that the films have a much-reduced superconducting transition (below 5 K), owing to the presence of traces of carbon and oxygen. However, we have recently demonstrated that thin films of NbN prepared by PAD undergo a superconducting transition at 12 K, similarly to films prepared by physical vapor deposition.[16]

Different scattering mechanisms can contribute to the resistivity of a conductor. The total resistivity $\rho(T)$ of the conductor may be expressed by Equation (1), where ρ_0 is the residual resistivity, T is the temperature, $\rho_{ph}(T)$ is the electron–phonon scattering, $\rho_{ee}(T)$ is the electron–electron scattering, and $\rho_m(T)$ is the scattering due to disordered localized magnetic moments.[15,17]

$$\rho(T) = \rho_0 + \rho_{ph}(T) + \rho_{ee}(T) + \rho_m(T) \quad (1)$$

Generally, electron–phonon scattering is prominent in the high-temperature region and follows a T^3 law according to Wilson's model for transition metals.[18] Electron–electron scattering is prominent in the low-temperature region, and scattering due to disordered localized magnetic moments is important at all temperatures; both follow a T^2 law.[19–21] Since all types of scattering follow power laws, Equation (2), where A and m are power-law parameters, is used to replace Equation (1).

$$\rho(T) = \rho_0 + A\,T^m \quad (2)$$

The values of m obtained by fitting Equation (2) to the data of Figure 4 can help us to understand the actual scattering mechanism that contributes to the resistivity of these ternary nitride samples. We found that the experimental resistivity data follow a T^2 variation in the low-temperature region from 5 to 80 K ($m = 2.02$ for BZN; $m = 2.03$ for BHN). However, the experimental resistivity data follow a T^3 variation in the intermediate-temperature region from 85 to 155 K ($m = 3.02$ for BZN; $m = 2.99$ for BHN). In the high-temperature region from 160 to 300 K, the value of m is 1.73 for BZN and 2.22 for BHN. It is reasonable to consider that electron–electron scattering is the main contribution to the resistivity at low temperatures and that electron–phonon scattering is the main contribution at intermediate temperatures. In the high-temperature region, the resistivity data for the ternary metal nitrides does not simply follow a T^2 or a T^3 variation, owing to competing contributions from electron–phonon scattering, scattering due to magnetic moments, and possibly other effects, such as scattering from the surfaces of the films.

It is well-known that the residual resistivity ratio (RRR = ρ_{300K}/ρ_{5K}) is a direct measure of film perfection. Values of RRR as large as 396 for BZN films and 203 for BHN films are obtained (with resistivities of 1.03×10^{-4} and $0.61 \times 10^{-4}\,\Omega$ cm at 300 K, respectively). Such large RRR values further

indicate that the epitaxial films grown by PAD are of nearly single-crystal quality, as the contributions from intragrain and intergrain scattering, as well as from scattering due to carbon and oxygen impurities, are very small.

In conclusion, the PAD approach allows the preparation of thin films of ternary nitrides. The epitaxial growth of phase-pure films of ternary nitrides makes it possible to study their intrinsic physical properties. BZN and BHN show metallic-like resistivity–temperature behavior from 5 to 300 K, with RRRs as large as 396 and 203, respectively.

Experimental Section

Sample preparation: To form epitaxial films of the ternary metal nitrides $BaZrN_2$ and $BaHfN_2$, solutions of the different metals (Ba, Zr, and Hf) and polymers were first prepared. Specifically, ethylenediaminetetraacetic acid (EDTA; 1 g) and polyethyleneimine (PEI; 1 g) were dissolved in water (25 mL). Barium nitrate (0.9 g) was then added to the solution. Using a similar process, metal–polymer solutions containing Zr and Hf were also prepared. Both PEI and EDTA were purchased from BASF (Clifton, NJ) and were used without further purification.

Ultrafiltration and concentration were carried out under 60 psi N_2 using Amicon stirred cells having a cut-off molecular weight of 3000. Metal analysis was conducted using a Varian Liberty 220 inductively coupled plasma atomic emission spectrometer (ICP-AES), following the standard SW846 Environmental Protection Agency (EPA) method 6010 procedure. After Amicon filtration, the final Ba, Zr, and Hf concentrations were 216, 101, and 94 mM, respectively.

Note that EDTA, in the PAD process, binds to metal ions through four carboxylate and two amine groups to form stable EDTA–metal complexes. The complexes further bind to PEI through a combination of hydrogen bonding and electrostatic attraction. In other words, the water-soluble polymer not only controls the viscosity of the process, but also binds the metal ions to prevent premature precipitation, resulting in a homogeneous distribution of the metal ions in the solution.

These metal–polymer solutions were then mixed to yield the desired stoichiometry (Ba/Zr = 1 for BZN; Ba/Hf = 1 for BHN). The homogeneous metal–polymer precursors were spin-coated onto single-crystal STO substrates. Finally, the precursor films were thermally treated under flowing ammonia gas at 1000 °C for 1 h to yield ternary metal nitride films.

Sample characterization: XRD was used to characterize the crystallographic orientation of the films. The microstructure of the films was analyzed by TEM. The surface morphology and surface roughness of the films were analyzed by SEM and AFM. RBS nuclear resonances at $^4He^+$ beam energies of 3.045 and 4.28 MeV were used to measure the oxygen and carbon contamination of the films, respectively. The transport properties of the films were evaluated using a physical property measurement system (PPMS).

Received: November 4, 2008
Published online: January 14, 2009

Keywords: nitrides · solution deposition · superconductors · thin films

[1] F. J. DiSalvo, *Science* **1990**, *247*, 649 – 655.
[2] N. E. Brese, M. O'Keeffe, *Struct. Bonding (Berlin)* **1992**, *79*, 307 – 378.
[3] F. J. DiSalvo, S. J. Clarke, *Curr. Opin. Solid State Mater. Sci.* **1996**, *1*, 241 – 249.
[4] R. Niewa, H. Jacobs, *Chem. Rev.* **1996**, *96*, 2053 – 2062.
[5] M. A. Sriram, K. S. Weil, P. N. Kumta, *Appl. Organomet. Chem.* **1997**, *11*, 163 – 179.
[6] R. Kniep, *Pure Appl. Chem.* **1997**, *69*, 185 – 191.
[7] R. Niewa, F. J. DiSalvo, *Chem. Mater.* **1998**, *10*, 2733 – 2752.
[8] O. Seeger, M. Hofmann, J. Strähle, J. P. Laval, B. Frit, *Z. Anorg. Allg. Chem.* **1994**, *620*, 2008 – 2013.
[9] D. H. Gregory, M. G. Barker, P. P. Edwards, M. Slaski, D. J. Siddons, *J. Solid State Chem.* **1998**, *137*, 62 – 70.
[10] D. H. Gregory, P. M. O'Meara, A. G. Gordon, D. J. Siddons, A. J. Blake, M. G. Barker, T. A. Hamor, P. P. Edwards, *J. Alloys Compd.* **2001**, *317–318*, 237 – 244.
[11] F. F. Lange, *Science* **1996**, *273*, 903 – 909.
[12] Q. X. Jia, T. M. McCleskey, A. K. Burrell, Y. Lin, G. E. Collis, H. Wang, A. D. Q. Li, S. R. Foltyn, *Nat. Mater.* **2004**, *3*, 529 – 532.
[13] A. K. Burrell, T. M. McCleskey, Q. X. Jia, *Chem. Commun.* **2008**, 1271 – 1277.
[14] L. E. Toth, *Transition Metal Carbides and Nitrides*, Academic Press, New York, **1971**.
[15] Y. Zhu, M. Ikeda, Y. Murakami, A. Tsukazaki, T. Fukumura, M. Kawasaki, *J. Appl. Phys.* **2007**, *46*, L1000 – L1002.
[16] G. F. Zou, M. Jain, H. Zhou, H. M. Luo, S. A. Baily, L. Civale, E. Bauer, T. Mark McCleskey, A. K. Burrell, Q. X. Jia, *Chem. Commun.* **2008**, 6022 – 6024.
[17] K. Lal, A. K. Meikap, S. K. Chattopadhyay, S. K. Chatterjee, M. Ghosh, K. Baba, R. Hatada, *Physica B* **2001**, *307*, 150 – 157.
[18] A. H. Wilson, *Proc. R. Soc. London Ser. A* **1938**, *167*, 580 – 593.
[19] N. V. Volkenshlein, V. P. Dyakina, V. E. Startsev, *Phys. Status Solidi B* **1973**, *57*, 9 – 42.
[20] P. A. Lee, T. V. Ramakrishnan, *Rev. Mod. Phys.* **1985**, *57*, 287 – 337.
[21] A. K. Meikap, S. K. De, S. Chatterjee, *Phys. Rev. B* **1994**, *49*, 1054 – 1063.

